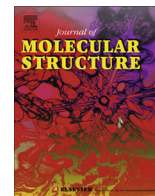




Contents lists available at ScienceDirect

Journal of Molecular Structure

journal homepage: www.elsevier.com/locate/molstruc

Practical crystal engineering using halogen bonding: A hierarchy based on calculated molecular electrostatic potential surfaces

Christer B. Aakeröy*, Tharanga K. Wijethunga, John Desper

Department of Chemistry, Kansas State University, Manhattan, KS 66506, USA

HIGHLIGHTS

- 36 co-crystallizations on compounds with two different acceptors were performed.
- An interaction hierarchy was established using calculated electrostatic potentials.
- All 10 structures obtained display best donor/acceptor halogen bonds.
- Halogen bonds with iodine are more effective than the bromo-analogues.

ARTICLE INFO

Article history:
Available online xxx

Keywords:
Halogen bond
Crystal engineering
Molecular recognition
Electrostatic potential
Co-crystallization
Hierarchy

ABSTRACT

A series of co-crystallization experiments were performed using four multi-topic N-heterocyclic acceptor molecules and nine aromatic halogen-bond donors in order to establish how effectively a ranking of bond strength based on calculated molecular electrostatic potential surfaces translates into predictable primary interactions in the solid state. A total of ten new crystal structures were obtained, and in each case, the observed interaction took place between the best acceptor (with the larger negative electrostatic potential) on the N-heterocycle and the halogen-bond donor. The supramolecular yield (number of successful co-crystallizations) is 70% for iodine-donors whereas none of the bromo-substituted donors produced a co-crystal which underscores the importance of the magnitude of the electrostatic potential and of the polarizability of the halogen-bond donor in the context of successful practical crystal engineering.

© 2014 Elsevier B.V. All rights reserved.

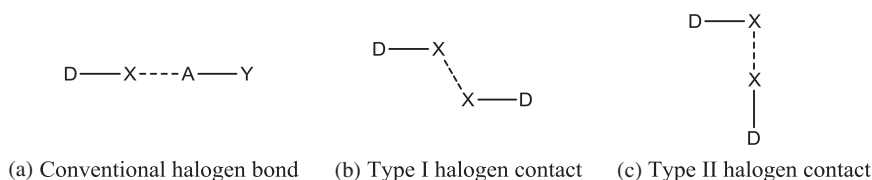
1. Introduction

Intermolecular interactions are responsible for all molecular recognition events, and as such represent the primary tools in supramolecular chemistry and crystal engineering [1]. Consequently, it is essential to have solid understanding of the fundamental nature of these interactions in order to successfully design complex supramolecules in a predetermined and effective manner [2–4]. Halogen bonds represent a relatively recent addition to the tool box of supramolecular chemistry and still receive considerable attention [5]. According to IUPAC, “A halogen bond R–X···Y–Z occurs when there is evidence of a net attractive interaction between an electrophilic region on a halogen atom X belonging to a molecule or a molecular fragment R–X (where R can be another atom, including X, or a group of atoms) and a nucleophilic region of a molecule, or molecular fragment, Y–Z” [6]. According to this definition the halogen-bond donor is accepting

electrons, a convention which is adopted to align it with the generally accepted definition of the hydrogen bond [7,8] where the electropositive hydrogen atom is recognized as the hydrogen-bond donor, accepting electrons from an electronegative atom [9]. The halogen bonding ability of donor atoms increase in the order of $F \ll Cl \ll Br < I$ depending on the polarizability [10], and conventional halogen bonds are highly directional [11]. Generally the bond distance between acceptor and donor atoms in a halogen bond is significantly shorter than the sum of van der Waals radii [12]. In addition to conventional stabilizing halogen bonds, two additional halogen···halogen contacts, classified as type I and type II (depending on the geometry) are frequently encountered in crystal structures of halogen-substituted molecules, Scheme 1 [13]. Factors that influence the strength of a halogen-bond include the presence of electron-withdrawing substituents that serve to ‘activate’ the halogen-bond donor atom by depleting it of electron density thereby increasing its partial positive potential [14,15].

In order to develop reliable and transferable synthetic guidelines for the assembly of molecular solids using multiple intermolecular interactions, Etter [16] and others [17–19] have

* Corresponding author. Tel.: +1 785 532 6096; fax: +1 785 532 6666.
E-mail address: aakeroy@ksu.edu (C.B. Aakeröy).



Scheme 1. (a) Conventional halogen bond (b) Type I halogen-halogen contact (c) Type II halogen-halogen contact; (D & Y-connected atoms, X-halogen bond donor atom, Y-halogen bond acceptor).

demonstrated that in hydrogen-bond based systems, there is a tendency for the best-donors to bind to the best-acceptors, and the second-best donor to bind to the second-best acceptor. If the molecules carry the same functionality, a relative ranking can be established reasonably well using pK_a/pK_b values [20–22] but if different functionalities are employed, an approach to ranking based on calculated molecular electrostatic potential surfaces is required [23–25].

At this point, it is not clear how effectively an electrostatic potential-based ranking of halogen-bond acceptors can be translated directly into strategies for practical crystal engineering, although a halogen bond donor based hierarchy [26], a basicity scale [27], ^{19}F NMR based studies [28], theoretical electrostatic based studies [5,29] and solution based models [30] have been used to explain halogen-bond interactions. In order to establish to what extent halogen bonds follow best-donor/best-acceptor guidelines, we decided to carry out systematic co-crystallizations on a series of N-heterocyclic halogen-bond acceptors, each with two binding sites with different electrostatic potential, Scheme 2, A1–A3. In addition, to ensure that the imidazole nitrogen atom was not inaccessible due to some steric hindrance, we also included ligand A4, with essentially the same shape, but with only one type of acceptor site. These four compounds have been co-crystallized with six iodo-substituted halogen-bond donors, D5–D10, (all but one of them ‘activated’ with fluorine groups) and three bromo-substituted halogen-bond donors, D11–D13, all of which are activated by a fluorinated aromatic backbone, Scheme 2. The study is undertaken in response to two hypotheses; (i) if a halogen-bond donor has a choice of two accessible halogen-bond acceptors, it will preferentially select the best-acceptor as determined by molecular electrostatic potentials surfaces (MEPS) and (ii) a bromo-substituted halogen-bond donor will be less successful at forming co-crystals than the corresponding iodo-analogues. The reactants were combined using solvent-assisted grinding, and the products were characterized using infrared spectroscopy. Successful experiments were then subjected to a variety of crystal-growth experiments and a total of ten samples produced crystals suitable for single-crystal diffraction.

2. Experimental

All the reagents, solvents, and donors D1–D9 and D11–D13 were purchased from commercial sources and used as received. 2,2′-Biimidazole was synthesized according to previously reported methods [31]. Donor D10 was prepared according to the synthetic methods reported [32]. A Fisher-Johns melting point apparatus was used to determine melting points. Infrared spectra were recorded with a Nicolet 380 FT-IR. 1H NMR spectra were recorded using a Varian Unity plus 400 MHz spectrometer.

2.1. Synthesis of 1,1′-bis(pyridin-4-ylmethyl)-2,2′-biimidazole, A1

2,2′-Biimidazole (0.27 g, 2 mmol) and NaOH (0.32 g, 8 mmol) were placed in a 100 mL round bottomed flask with 20 mL of acetonitrile. The mixture was stirred at room temperature for two hours. 4-Picolyl chloride hydrochloride (0.65 g, 4 mmol) in acetoni-

trile (20 mL) was added to the mixture and refluxed for 24 h at 50–60 °C. The reaction was monitored with TLC and after completion the solvent was removed by rotary evaporation. The residue was dissolved in water (50 mL) and extracted with methylene chloride (30 mL \times 3). Organic layers were combined, dried over anhydrous $MgSO_4$ and rotary evaporated to obtain the dark brown color powder as the product. Yield: 0.35 g (56%); mp 157–160 °C; 1H NMR (δ_H ; $CDCl_3$, 400 MHz): 8.49 (d, 4H), 7.11 (d, 2H), 6.94 (d, 2H), 6.91 (d, 4H), 5.84 (s, 4H).

2.2. Synthesis of 1,1′-bis(pyridin-3-ylmethyl)-2,2′-biimidazole, A2

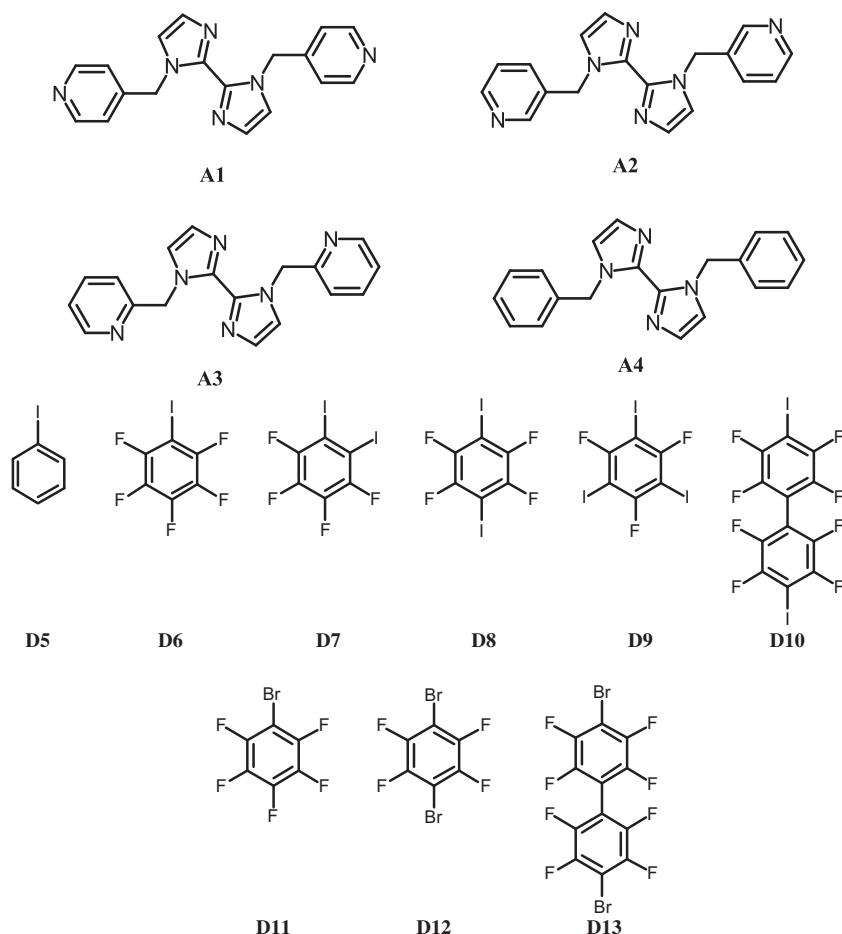
2,2′-Biimidazole (0.27 g, 2 mmol) and NaOH (0.32 g, 8 mmol) were placed in a 100 mL round bottomed flask with 20 mL of acetonitrile. The mixture was stirred at room temperature for two hours. 3-Picolyl chloride hydrochloride (0.65 g, 4 mmol) in acetonitrile (20 mL) was added to the mixture and refluxed for 24 h at 50–60 °C. The reaction was monitored with TLC and upon completion the solvent was removed by rotary evaporation. The residue was dissolved in water (50 mL) and extracted with methylene chloride (30 mL \times 3). Organic layers were combined, dried over anhydrous $MgSO_4$ and rotary evaporated to obtain the brown color powder as the product. Yield: 0.45 g (71%); mp 112–115 °C; 1H NMR (δ_H ; $CDCl_3$, 400 MHz): 8.46 (d, 2H), 8.45 (s, 2H), 7.39 (d, 2H), 7.17 (m, 2H), 7.11 (d, 2H), 6.95 (d, 2H), 5.78 (s, 4H).

2.3. Synthesis of 1,1′-bis(pyridin-2-ylmethyl)-2,2′-biimidazole, A3

2,2′-Biimidazole (0.27 g, 2 mmol) and NaOH (0.32 g, 8 mmol) were placed in a 100 mL round bottomed flask with 20 mL of acetonitrile. The mixture was stirred at room temperature for two hours. 2-Picolyl chloride hydrochloride (0.65 g, 4 mmol) in acetonitrile (20 mL) was added to the mixture and refluxed for 24 h at 50–60 °C. The reaction was monitored with TLC and upon completion the solvent was removed by rotary evaporation. The residue was dissolved in water (50 mL) and extracted with methylene chloride (30 mL \times 3). Organic layers were combined, dried over anhydrous $MgSO_4$ and rotary evaporated to obtain the pale brown color powder as the product. Yield: 0.25 g (40%); mp 180–183 °C; 1H NMR (δ_H ; $CDCl_3$, 400 MHz): 8.53 (d, 2H), 7.53 (t, 2H), 7.15 (t, 2H), 7.12 (s, 2H), 7.07 (s, 2H), 7.05 (d, 2H), 5.87 (s, 4H).

2.4. Synthesis of 1,1′-dibenzyl-2,2′-biimidazole, A4

2,2′-Biimidazole (0.33 g, 2.48 mmol) and NaOH (0.39 g, 9.92 mmol) were placed in a 100 mL round bottomed flask with 20 mL of acetonitrile. The mixture was stirred at room temperature for two hours. Benzyl bromide (0.63 g, 5 mmol) in acetonitrile (20 mL) was added to the mixture and refluxed for 24 h at 50–60 °C. The reaction was monitored with TLC and after completion the solvent was removed by rotary evaporation. The residue was dissolved in water (50 mL) and extracted with methylene chloride (30 mL \times 3). Organic layers were combined, dried over anhydrous $MgSO_4$ and rotary evaporated to obtain the yellow color powder as the product. Yield: 0.69 g (89%); mp 144–146 °C; 1H NMR (δ_H ;



Scheme 2. Halogen-bond acceptors (**A1–A4**) and halogen-bond donors (**D5–D13**) in this study.

Table 1

Values of electrostatic potentials of acceptors and donors.

	Molecule	Atom	(kJ/mol)
Acceptors	1,1'-Bis(pyridin-4-ylmethyl)-2,2'-biimidazole A1	Pyridine N	–187
		Imidazole N	–132
	1,1'-Bis(pyridin-3-ylmethyl)-2,2'-biimidazole A2	Pyridine N	–182
		Imidazole N	–128
	1,1'-Bis(pyridin-2-ylmethyl)-2,2'-biimidazole A3	Pyridine N	–153
	Imidazole N	–125	
	1,1'-Bibenzyl-2,2'-biimidazole A4	Imidazole N	–149
Donors	Iodobenzene D5	Iodine	+103
	Iodopentafluorobenzene D6	Iodine	+166
	1,2-Diiodotetrafluorobenzene D7	Iodine	+162
	1,4-Diiodotetrafluorobenzene D8	Iodine	+169
	1,3,5-Triiodotrifluorobenzene D9	Iodine	+158
	4,4'-Diiodoperfluorobiphenyl D10	Iodine	n/a
	Bromopentafluorobenzene D11	Bromine	+143
	1,4-Diiodotetrafluorobenzene D12	Bromine	+139
	4,4'-Dibromoperfluorobiphenyl D13	Bromine	n/a

CDCl₃, 400 MHz): 5.70 (s, 4H), 6.93 (d, 2H), 7.03 (m, 4H), 7.12 (d, 2H), 7.24 (m, 6H).

2.5. Molecular electrostatic potential calculations

Electrostatic potentials on the acceptor molecules were calculated with density functional B3LYP level of theory with 6-31G^{*} basis set in vacuum. Electrostatic potentials on donor molecules were calculated with density functional B3LYP level of theory

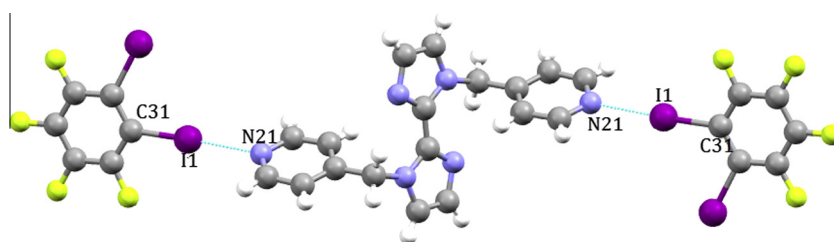
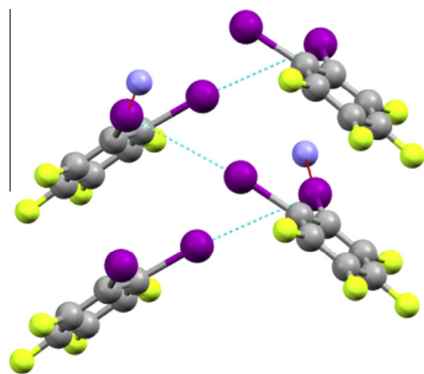
using 6-311++G^{**} basis set in vacuum. Calculations for **D10** and **D13** could not be done using this level of theory. All calculations were carried out using Spartan 8 software.

2.6. Grinding experiments

The initial screening was carried out using solvent-assisted grinding (methanol). Each combination of acceptors and donors were mixed in specific stoichiometries (see [Supplementary](#)

Table 2
Halogen-bond geometries.

Co-crystal	C–I...N	N...I (Å)	N...I–C (^o)
A1D7	C(31)–I(1)...N(21)	2.7777(18)	177.06(6)
A1D8	C(31)–I(1)...N(11)	2.7913(14)	175.98(5)
A1D10	C(31)–I(1)...N(21)	2.7747(13)	173.45(5)
A2D7	C(31)–I(1)...N(21) C(32)–I(2)...N(21)	2.848(5) 3.255(5)	174.39(19) 165.16(18)
A2D8	C(31)–I(1)...N(21)	2.8598(13)	175.13(5)
A2D9	C(312)–I(42)...N(212) C(311)–I(11)...N(211) C(332)–I(52)...N(132)	2.757(2) 2.830(2) 3.123(2)	176.06(8) 176.70(8) 164.81(7)
A2D10	C(31)–I(1)...N(21) C(41)–I(2)...N(13)	2.824(2) 3.1345(19)	175.93(7) 166.07(7)
A3D9	C(33)–I(2)...N(21)	2.887(3)	178.09(10)
A3D10	C(31)–I(1)...N(21) C(41)–I(2)...N(13)	2.8813(16) 3.3015(17)	175.87(6) 164.27(6)
A4D9	C(511)–I(11)...N(131) C(512)–I(42)...N(132)	2.897(4) 3.028(4)	174.13(16) 171.17(19)

**Fig. 1.** Primary halogen bond interactions in the co-crystal **A1D7**.**Fig. 2.** Secondary interactions in co-crystal **A1D7**.

Information for details) and the solid resulting from each reaction was characterized by IR spectroscopy. Successful interactions between the acceptor and donor were identified using the specific shifts of the peaks of the mixture compared to starting compounds.

2.7. Synthesis of co-crystals

The resulting mixtures used in the grinding experiments were dissolved in a minimum amount of methanol and kept in a vial for slow evaporation in order to obtain co-crystals suitable for single crystal X-ray diffraction (see [Supplementary Information](#) for details). Once the crystals were obtained they were again analyzed using IR spectroscopy and melting point and subjected to single-

crystal X-ray diffraction. Experimental details for grinding and slow evaporations with specific IR shifts are recorded in the ESI.

2.8. X-ray crystallography

Datasets were collected at 120 K on a Bruker Kappa APEX II system with Cu radiation (A2D7) or a Bruker SMART APEX II system with Mo radiation at 120 K (the remainder) using APEX2 software. An Oxford Cryostream 700 low-temperature device was used to control temperature. MoK radiation was used. Initial cell constants were found by small widely separated “matrix” runs. Data collection strategies were determined using COSMO. Scan speeds and scan widths were chosen based on scattering power and peak rocking curves. Unit cell constants and orientation matrices were improved by least-squares refinement of reflections thresholded from the entire dataset. Integrations were performed with SAINT, using these improved unit cells as a starting point. Precise unit cell constants were calculated in SAINT from the final merged datasets. Lorentz and polarization corrections were applied. Absorption corrections were applied using SADABS. Datasets were reduced with SHELXTL. The structures were solved by direct methods without incident. All hydrogen atoms were assigned to idealized positions and were allowed to ride. Isotropic thermal parameters for the hydrogen atoms were constrained to be $1.5 \times (\text{methyl})/1.2 \times$ (all other) that of the connected atom. CCDC 966785–966794 contains the [supplementary crystallographic data](#) for this paper. These data can be obtained free of charge via <http://www.ccdc.cam.ac.uk/conts/retrieving.html> (or from the Cambridge Crystallographic Data Centre, 12, Union Road, Cambridge CB2 1EZ, UK; fax:+44 1223 336033).

3. Results

The ranking of acceptor sites was based on the calculated molecular electrostatic surface potentials, Table 1. Once the initial screen was completed using IR spectroscopy, ten co-crystals produced crystals suitable for single crystal X-ray diffraction. The experimental crystallographic data are found in the ESI (Table S3) and the halogen-bond geometries are listed in Table 2.

Ten crystal structures were obtained (A1D7, A1D8, A1D10, A2D7, A2D8, A2D9, A2D10, A3D9, A3D10 and A4D9) and subsequently analyzed to determine binding preferences between donors and ditopic acceptors.

The crystal structure of A1D7 displays the expected 1:2 stoichiometry where one acceptor molecule interacts with two donor molecules forming a discrete trimer, Fig. 1. The primary halogen bonds take place between one of the two iodine atoms and the N-pyridine moiety (the best acceptor) whereas the second iodine

atom is involved in a Type II close contact with an iodine atom from a neighboring donor molecule, Fig. 2.

The crystal structure of A1D8 (with a 1:1 stoichiometry) contains infinite 1-D chains constructed from I...N(py) halogen bonds, Fig. 3. The imidazole nitrogen atoms do not compete for halogen bonds and instead form short contacts with C–H moieties of a neighboring acceptor molecule, Fig. 4, resulting in a stacking of adjacent chains, Fig. 4.

The co-crystal A1D10 has 1:2 stoichiometry (donor:acceptor) and contains discrete trimers as the second iodine atom does not participate in a halogen bond. Again, the best acceptor, N(py) is the preferred binding site, Fig. 5. Unlike in the crystal structure of A1D8, imidazole nitrogen atoms not participating in any notable secondary interactions, while the second iodine of each donor molecule is not participating in any considerable interactions as well.

The crystal structure of A2D7 reveals a 1:1 stoichiometry. This time, the best-acceptor, N(py) forms a bifurcated halogen bond, Fig. 6, which in turn results in chains of tetrameric-rectangles.

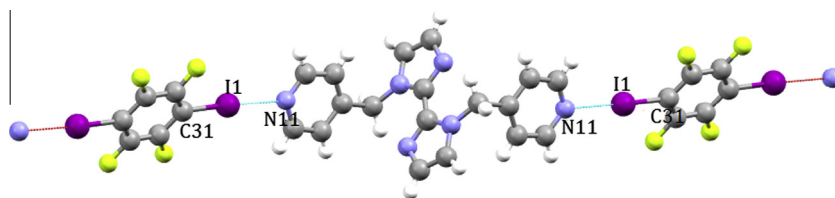


Fig. 3. Formation of infinite chains via halogen bonds in A1D8.

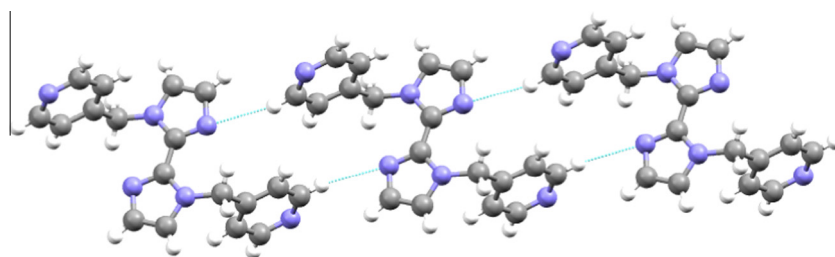


Fig. 4. Secondary interactions in A1D8.

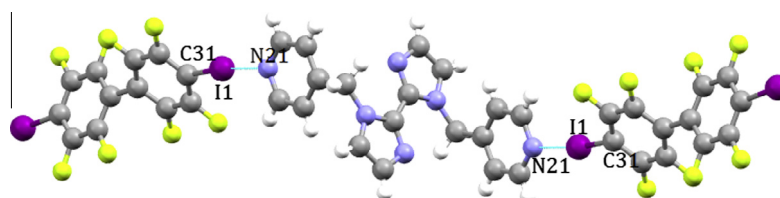


Fig. 5. A trimer in co-crystal A1D10.

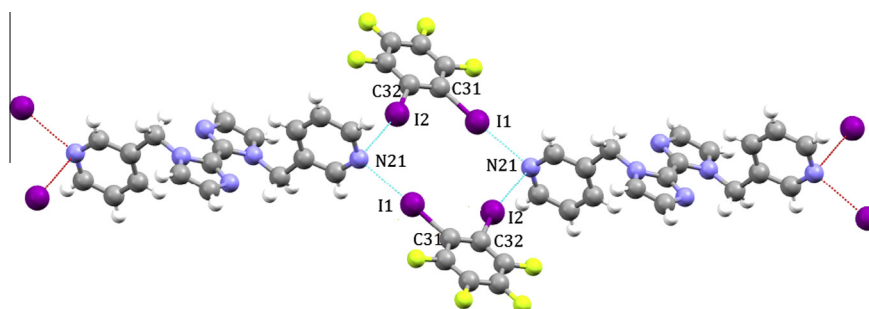


Fig. 6. Primary halogen bond interaction in A2D7.

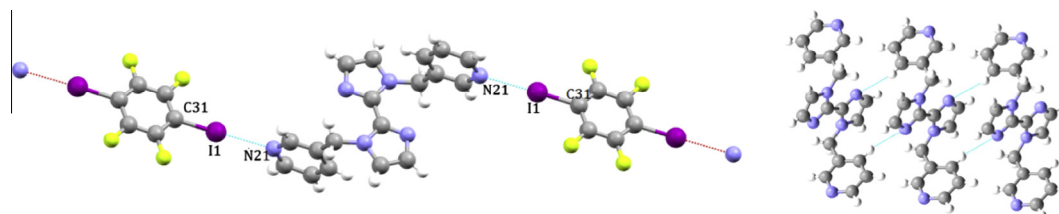


Fig. 7. Primary and secondary interactions in **A2D8**.

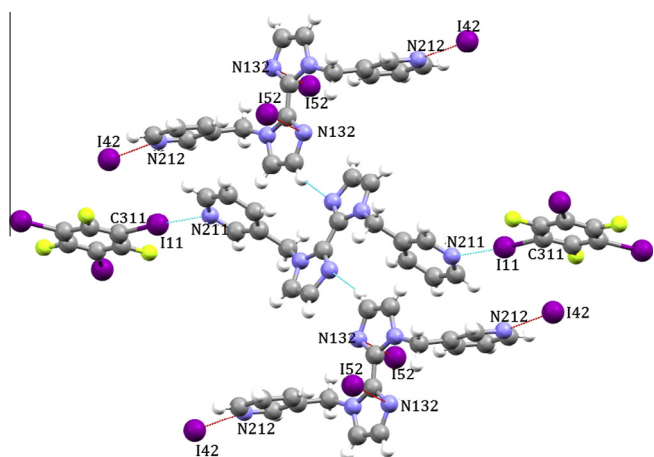


Fig. 8. A halogen-bond based trimer and secondary C–H...N(im) interactions in **A2D9**.

No notable secondary interactions are found with the imidazole nitrogen atoms.

The crystal structure of **A2D8** has a 1:1 stoichiometry and contains 1-D chains and C–H...N(im) contacts similarly to what was observed in the structure of **A1D8**, Fig. 7.

The crystal structure of **A2D9** also displays a 1:1 stoichiometry and two distinct halogen-bond motifs are present. First, a trimer assembled via a I...N(py) (best-acceptor) halogen bond, Fig. 8, and second, intermolecular C–H...N(im) hydrogen bonds that connect neighboring acceptor molecules. The latter event leads to

'chains of hexamers' where all four nitrogen atoms form halogen bonds, Fig. 9. The third iodine atom of the donor molecule is inactive (which is not uncommon) [33,34].

The crystal structure determination of **A2D10** shows that the donor and acceptor molecules appear in a 1:2 stoichiometry, where all four nitrogen atoms are participating in halogen bonds leading to infinite ribbons, Fig. 10.

The co-crystal **A3D9** has a stoichiometry of 1:1 and contains 1-D chains assembled using C–I...N(py) halogen bonds, Fig. 11. The imidazole nitrogen atoms and third iodine atom do not have any significant short contacts.

The structure determination of **A3D10** shows that the acceptor and donor are present in a 1:2 stoichiometry and, similarly to the structure **A2D10**, contains chains of rectangles using all four nitrogen atoms on the acceptor, Fig. 12.

In the 1:1 co-crystal of **A4D9**, the 'arms' of the acceptor are, unexpectedly, both appearing on the same face of the aromatic core of **A4**. In addition, one of the N(im) nitrogen atoms form a conventional, near-linear halogen bond, whereas the other nitrogen atom forms a bifurcated halogen bond with two adjacent donor molecules. Interestingly, all three iodine atoms of the donor participate in halogen bonds which is unique in this series of crystal structures, Fig. 13.

4. Discussion

Thirty-six co-crystallizations involving four bis-pyridine/bis-imidazole based acceptor molecules and nine aromatic halogen-bond donors were performed in order to determine to what extent co-crystallizations driven by halogen-bond interactions follow the same best-donor/best-acceptor rules (where the ranking is based

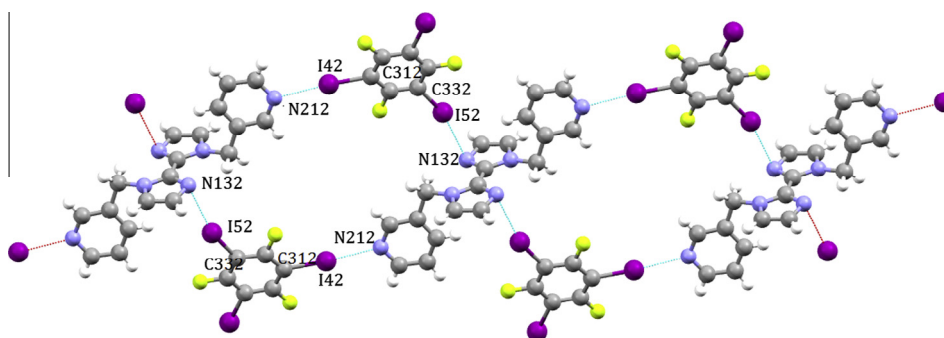


Fig. 9. A chain of hexagons in the crystal structure of **A2D9**.

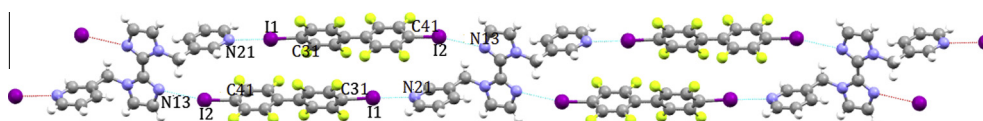


Fig. 10. An infinite ribbon in **A2D10**.

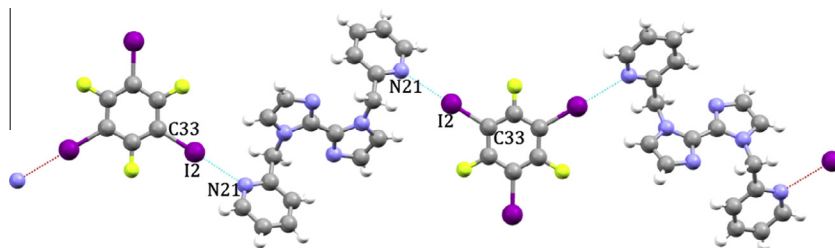


Fig. 11. Primary halogen bond interactions in co-crystal **A3D9**.

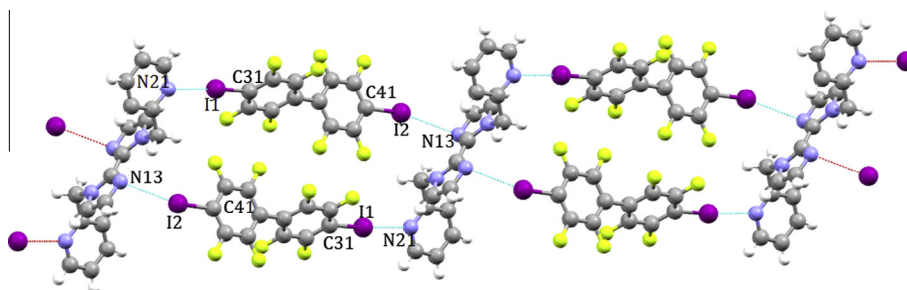


Fig. 12. Chain of rectangles in the structure of **A3D10**.

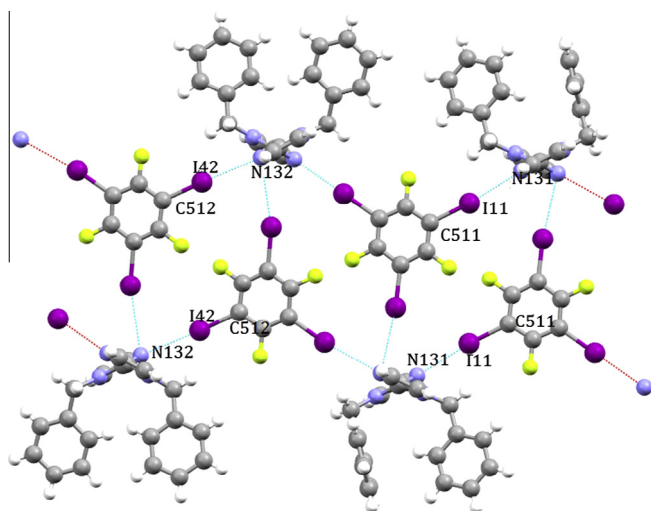


Fig. 13. Halogen bond interactions in the structure of **A4D9**.

on electrostatics) as are hydrogen bonds. The three ditopic acceptors **A1**–**A3** have two acceptor sites that differ primarily by their electrostatic potentials; N(py) occupies a more negative site than N(im) making it the better acceptor. In order to ensure that any observed binding preferences were not simply the result of steric hindrance, we also included an acceptor **A4** which only contains imidazole sites in the same steric environment as in **A1**–**A3**. The ranking and hierarchy of the acceptor sites was established using DFT calculated MEPS, Table 1. The calculations indicate that the pyridine nitrogen atom carries a higher partial negative electrostatic potential (EP) than the imidazole nitrogen atom and is thus ranked as the ‘best’ acceptor site.

The grinding experiments showed a pronounced positive correlation between the EP on the acceptor sites and the supramolecular yield (the percentage of successful reactions) again indicating that the magnitude of the electrostatic potential plays a major role in ranking the relative strength and efficiency of competing halogen-bond sites, Table 3. In Table 3, the success rates are the num-

ber of experiments with positive results (co-crystal formation), while supramolecular yields are the success percentage relative to the total number of experiments in each category.

The electrostatic potentials associated with the N(py) atoms of **A1** and **A2** are close, and their success rates are also similar. Upon moving from **A1** to **A4** the magnitudes of the negative EPs on the nitrogen atoms decrease and their success rates are also decreasing. Although the number of data points is rather small, the trend is consistent with previously reported results, [29] and show that the magnitude of the electrostatic potential plays a key role when determining the likelihood that a particular combination of donor and acceptor sites will interact strongly enough to drive the formation of a co-crystal. There is a dramatic difference in halogen-bond ability between iodo- and bromo substituted compounds which reflect the polarizability, MEPS and size/depth of the respective σ -hole; the former have a 70% supramolecular yield, whereas none of the bromo-substituted donors produced co-crystals. On the other hand the control experiments with iodobenzene showed that the ‘activation’ offered by electron-withdrawing fluorine substituents is crucial to the ability of a halogen atom to form halogen bonds of real supramolecular relevance, again consistent with theory [5].

An examination of all ten crystal structures clearly demonstrate that, given a choice, a strong halogen-bond donor preferentially interacts with an acceptor atom with a more negative electrostatic potential, which shows that practical halogen-bond selectivity follows a best-donor/best acceptor guideline. In the three structures where the imidazole nitrogen also participated in a halogen bond, **A3D10**, **A2D10** and **A2D9**, the N(im)···I distances were substantially longer than the N(py)···I length which gives an indication that the former are less favorable than the latter. Furthermore, an N(im)···I halogen bond did not appear in structures with **A1**, wherein the N(py) atom has a substantially more negative electrostatic potential, relative to the N(im) atom, than in **A2** and **A3**.

Acceptor **A4** was used as a control experiment to ensure that the imidazole nitrogen atoms are in fact sterically accessible for halogen bond formation and, consequently, not less competitive due to some form of steric hindrance. In cases when all four nitrogen atoms participate in halogen bonds, it has resulted in the

Table 3
Supramolecular yields.

	A1	A2	A3	A4
EP (in kJ/mol)	N _{pyridine} (−187) N _{imidazole} (−132)	N _{pyridine} (−182) N _{imidazole} (−128)	N _{pyridine} (−153) N _{imidazole} (−125)	– N _{imidazole} (−149)
Success rate – grinding	5/9	5/9	4/9	3/9
Success rate – slow evaporation	4/9	4/9	3/9	2/9
Total supramolecular yield	55%	55%	45%	33%
Success rate with iodine donors – grinding	5/6	5/6	4/6	3/6
Supramolecular yield with iodine donors	83%	83%	67%	50%
Total supramolecular yield = 47%				
Total supramolecular yield with iodine donors = 70%				
Total supramolecular yield with bromine donors = 0%				

formation architectures comprising polygonal architectures such as rectangles (**A3D10** and **A2D10**) and hexagonal motifs (**A2D9**).

In **A2D7** and **A4D9** the nitrogen atoms are participating in dissymmetric bifurcated halogen bonds, where one of the contacts is shorter than the other. Such halogen bonds are rare, as nitrogen atoms, with only one lone pair, tend to be satisfied with a single electron-pair acceptor forming one non-covalent interaction only.

If we consider the donor molecules in these ten co-crystal structures various behaviors can be recognized. In **A1D7**, one of the iodine atoms of halogen bond donor is participating in forming a Type II halogen bond where the electropositive tip of the iodine atom is interacting with the electronegative region of the another iodine atom. In **A1D10**, even though the two iodine atoms in donor **D10** should have the same initial strength (due to the symmetry of the molecule), the second iodine atom is not participating in any interactions leading to a trimer formation in this case. It should be pointed out that it is not possible to fully rationalize or predict every structural aspect of the solid state through an examination that focuses on relatively strong and directional intermolecular interactions such as hydrogen- and halogen bonds. Although these forces are clearly capable of, and responsible for, the bringing together of different neutral molecular within the same crystalline solid, but the detailed outcome of nucleation and crystallization is also influenced by weaker non-covalent interactions.

5. Conclusion

This study highlights the importance of using calculated molecular electrostatic potentials as a way of ranking the relative efficiency of specific halogen-bond interactions in solid-state architectures where multiple binding options are available between the reactants. In fact, halogen bonds seem to reflect the previously established propensity of hydrogen-bonds for following a best-donor best-acceptor interaction hierarchy in the solid state. In all ten crystal structures that were obtained in this study, halogen bonds involving the “better” acceptor are favored.

Appendix A. Supplementary material

Supplementary data associated with this article can be found, in the online version, at <http://dx.doi.org/10.1016/j.molstruc.2014.02.022>.

References

- [1] J.M. Lehn, *Chem. Soc. Rev.* 36 (2007) 151.
- [2] J.B. Benedict, *Recent Adv. Crystallogr.* (2012). InTech.
- [3] F. Meyer, P. Dubois, *CrystEngComm* 15 (2013) 3058.
- [4] D. Cincič, T. Friščič, W. Jones, *Chem. Eur. J.* 14 (2008) 747.
- [5] (a) P. Metrangolo, F. Meyer, T. Pilati, G. Resnati, G. Terraneo, *Angew. Chem. Int. Ed.* 47 (2008) 6114;
(b) M. Erdelyi, *Chem. Soc. Rev.* 41 (2012) 3547;
(c) T.M. Beale, M.G. Chudzinski, M.G. Sarwar, M.S. Taylor, *Chem. Soc. Rev.* 42 (2013) 1667;
(d) P. Politzer, J.S. Murray, *ChemPhysChem* 14 (2013) 278;
(e) P. Politzer, J.S. Murray, T. Clark, *Phys. Chem. Chem. Phys.* 15 (2013) 11178.
- [6] G.R. Desiraju, S. Ho, L. Kloo, A.C. Legon, R. Marquardt, P. Metrangolo, P.A. Politzer, G. Resnati, K. Rissanen, *IUPAC Provisional Recommendation*.
- [7] A. Priimagi, G. Cavallo, P. Metrangolo, G. Resnati, *Acc. Chem. Res.* 46 (2013) 2686.
- [8] S. Tothadi, G.R. Desiraju, *Chem. Commun.* 49 (2013) 7791.
- [9] T. Steiner, *Angew. Chem. Int. Ed.* 41 (2002) 48.
- [10] J. Lieffrig, O. Jeannin, A. Frączkowiak, I. Olejniczak, R. Świetlik, S. Dahaoui, E. Aubert, E. Espinosa, P.A. Senzier, M. Fourmigu, *Chem. Eur. J.* 19 (2013) 14804.
- [11] P. Politzer, J.S. Murray, T. Clark, *Phys. Chem. Chem. Phys.* 12 (2010) 7748.
- [12] P. Metrangolo, H. Neukirch, T. Pilati, G. Resnati, *Acc. Chem. Res.* 38 (2005) 386.
- [13] G.R. Desiraju, R. Parthasarathy, *J. Am. Chem. Soc.* 111 (1989) 8725.
- [14] P. Metrangolo, G. Resnati, *Chem. Eur. J.* 7 (2001) 2511.
- [15] A. Bauzá, D. Quin-ones, A. Frontera, P.M. Deyà, *Phys. Chem. Chem. Phys.* 13 (2011) 20371.
- [16] M.C. Etter, *Acc. Chem. Res.* 23 (1990) 120.
- [17] J.R. Bowers, G.W. Hopkins, G.P.A. Yap, K.A. Wheeler, *Cryst. Growth Des.* 5 (2005) 727.
- [18] C.B. Aakeröy, A.M. Beatty, B.A. Helfrich, *Angew. Chem. Int. Ed.* 40 (2001) 17.
- [19] G.R. Desiraju, J.J. Vittal, A. Ramanan, *Crystal Engineering: A Textbook*, World Scientific, 2011.
- [20] D.E. Lynch, P. Sandhu, S. Parsons, *Aust. J. Chem.* 53 (2000) 383.
- [21] C.B. Aakeröy, A.M. Beatty, B.A. Helfrich, *Angew. Chem. Int. Ed.* 17 (2001) 3240.
- [22] K.S. Huang, D. Britton, M.C. Etter, S.R. Byrn, *J. Mater. Chem.* 7 (1997) 713.
- [23] C.A. Hunter, *Angew. Chem. Int. Ed.* 43 (2004) 5310.
- [24] P.W. Kenny, *J. Chem. Inf. Model.* 49 (2009) 1234.
- [25] C.B. Aakeröy, K.N. Epa, F. Forbes, J. Desper, *CrystEngComm* 15 (2013) 5946.
- [26] C.B. Aakeröy, M. Baldrighi, J. Desper, P. Metrangolo, G. Resnati, *Chem. – A Eur. J.* 19 (2013) 16240.
- [27] J.Y.L. Questel, C. Laurence, J. Graton, *CrystEngComm* 15 (2013) 3212.
- [28] M.G. Sarwar, B. Dragisic, L.J. Salsberg, C. Gouliaras, M.S. Taylor, *J. Am. Chem. Soc.* 132 (2010) 1646.
- [29] K.E. Riley, P. Hobza, *Phys. Chem. Chem. Phys.* 15 (2013) 17742.
- [30] Y. Lu, H. Li, X. Zhu, W. Zhu, H. Liu, *J. Phys. Chem. A* 115 (2011) 4467.
- [31] J. Xiao, J.M. Shreeve, *J. Org. Chem.* 8 (2005) 3072.
- [32] G.M. Espallargas, A. Recuenco, F.M. Romero, L. Brammer, S. Libri, *CrystEngComm* 14 (2012) 6381.
- [33] C.B. Aakeröy, T.K. Wijethunga, J. Desper, *CrystEngComm* 16 (2014) 28–31.
- [34] A.C.B. Lucassen, A. Karton, G. Leitens, L.J.W. Shimon, J.M.L. Martin, M.E. van der Boom, *Cryst. Growth Des.* 7 (2007) 386.